AJNR

Correlation between Lumenal Geometry Changes and Hemodynamics in Fusiform Intracranial Aneurysms

Liang-Der Jou, Gregory Wong, Brad Dispensa, Michael T. Lawton, Randall T. Higashida, William L. Young and David Saloner

AJNR Am J Neuroradiol 2005, 26 (9) 2357-2363
http://www.ajnr.org/content/26/9/2357

Correlation between Lumenal Geometry Changes and Hemodynamics in Fusiform Intracranial Aneurysms

Liang-Der Jou, Gregory Wong, Brad Dispensa, Michael T. Lawton, Randall T. Higashida, William L. Young, and David Saloner

BACKGROUND AND PURPOSE: **Hemodynamics may predispose aneurysms to rupture; however, hemodynamic descriptors that can describe aneurysm growth are not well understood. We examined the relationship between hemodynamics and growth of 2 fusiform basilar artery aneurysms in an effort to define hemodynamic variables that may be helpful in predicting aneurysmal growth.**

METHODS: **Two patients with basilar fusiform aneurysms of a similar size were followed for a 2-year period. The lumenal geometry and inflow and outflow rates were acquired by using MR angiography and velocimetry, respectively. The location of aneurysmal growth was identified by coregistering aneurysm models that were acquired at different times. Hemodynamic descriptors were calculated by using computational fluid dynamic simulations and compared with aneurysm growth pattern.**

RESULTS: **One patient had an aneurysm that grew significantly, but a similar-sized aneurysm in the other patient remained unchanged. The largest aneurysmal growth (~3 mm/year) was found at the inferior side (lower part) of the aneurysm, where the wall shear stress was very low ($<0.1 N/m^2$). The general flow patterns did not change with time, even in the aneurysm that grew, but histograms of wall shear stress were very different in these 2 patients.**

CONCLUSIONS: **This study investigates whether hemodynamic descriptors can be correlated with regional changes in aneurysm lumen morphology on a patient-specific basis. That capability will permit the testing, in longitudinal studies, of hypotheses as to which mechanisms are the most important in aneurysm growth.**

It has long been maintained that hemodynamic forces play an important role in determining the location, rate of growth, and ultimate rupture of aneurysms. Flow in fusiform aneurysms is highly complex, and there are a number of important hemodynamic variables that can be used to characterize these flow patterns, such as pressure, wall shear stress, and the location of a flow impingement zone. The relative importance of these descriptors remains speculative, because there is a paucity of data that confirms a positive relationship between any of those descriptors and observed changes in aneurysm morphology. This applies both to the natural history of untreated aneurysms and to those who have undergone surgical or endovascular treatment (1, 2). A previous study indicated that the growth of a vertebrobasilar aneurysm coincided with the location of high hemodynamic impact following intervention (1). The increase of pressure, however, was only ~4 mmHg, which is considerably less than the pressure variation between systole and diastole (3). Therefore, whether flow impingement or local elevated wall shear is responsible for the growth of an aneurysm remains controversial (1, 4). Establishing the precise role of flow dynamics on aneurysm progression would provide important insights into the underlying physiology and could be useful in steering interventions.

Computational fluid dynamic simulations of the flow in vascular structures require a definition of the lumenal geometry and the inflow and outflow values. Models of the lumenal geometry can be readily extracted from 3D data sets acquired in vivo such as MR angiograms (1, 5–7) or rotational conventional

Received January 24, 2005; accepted after revision April 28.

From the Departments of Radiology (L.D.J., G.W., R.T.H., D.S.), Neurological Surgery (M.T.L., R.T.H., W.L.Y.), Anesthesia and Perioperative Care (B.D., R.T.H., W.L.Y.), and Neurology (R.T.H., W.L.Y.), University of California–San Francisco, San Francisco, CA.

Address correspondence to Liang-Der Jou, PhD, McGowan Institute for Regenerative Medicine and Department of Radiology and Bioengineering, University of Pittsburgh, 3025 E. Carson St., Pittsburgh, PA 15203.

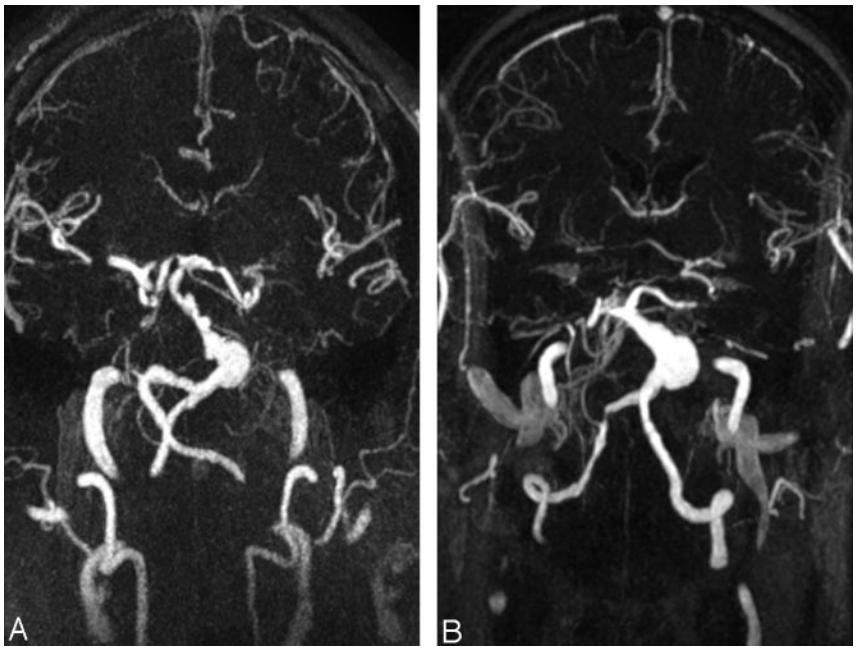

FIG 1. MIPS images of a stable and growing aneurysm.

radiographic angiography images (5), and MR imaging can also provide flow velocities. A number of numerical algorithms have been developed to generate patient-specific vascular models (5, 8–10). These imaged-based models permit an evaluation of cerebral aneurysms on an individual basis and allow us to examine anatomic and physiologic differences between different models. In this study, we demonstrate the differences in intra-aneurysmal hemodynamics between 2 patients, one with a growing aneurysm and the other with a stable aneurysm that has not presented any change of aneurysmal volume. The hemodynamic conditions for these aneurysms were quantified and compared.

Case Presentations

Eleven subjects were recruited to join this study. The recruitment of these patients followed a protocol approved by the institutional review board at our institution. In each case, because of poor therapeutic options, a clinical decision was made to leave the aneurysm untreated. These individuals were imaged on an annual basis between 2002 and 2004. These subjects have marked variation in the geometry of their aneurysms. Of this cohort, 5 patients had aneurysms at their basilar trunks. Two patients had geometries that were quite similar—bulbous aneurysms in the proximal segment of the basilar artery and similar size (~15 mm). Three other aneurysms were either >20 mm or <12 mm. These 2 cases were selected for a rigorous comparison of the predicted flow fields and size progression and are reported here.

Case 1

A 59-year-old man was diagnosed with a pituitary adenoma in 1995. At the time of evaluation, he was also diagnosed with a fusiform basilar artery aneurysm and an aneurysm at his middle cerebral artery (Fig 1*A*). The aneurysm near the vertebral junction was measured to be 15 mm in width and 15 mm in length. The patient had not been symptomatic from either of his 2 cerebral aneurysms. He was otherwise in good health, with no other major health problems and no focal neurologic deficits; thus, a conservative management plan was chosen.

Case 2

A 70-year-old man presented with an episode suggestive of a posterior circulation transient ischemia attack. He had a normal neurologic examination, but was hypertensive. Digital subtraction angiography demonstrated a fusiform, lobulated aneurysm of the basilar artery involving the basilar artery beginning just distal to the vertebrobasilar junction and extending to the distal basilar artery, proximal to the origins of the superior cerebellar arteries (Fig 1*B*). The aneurysm was eccentric to the left, with an axial diameter of 10.6 mm and a length of 8.7 mm in 2002, but it grew significantly to an axial diameter of 13.3 mm by 2003. Of note, there was a severe focal stenosis of the right vertebral artery distal to the posterior inferior cerebellar artery origin, consistent with atherosclerotic disease. He was managed with aspirin and has not had further symptoms. There was mass effect on the pons and medulla.

Image Acquisition and Analysis

Patients were imaged with contrast-enhanced MR angiography with image parameters of 5 ms/1.6 ms/1 (TR/TE/NEX); flip angle of 30°, interpolated matrix size of 512 × 512, and field of view of 20 cm on a 1.5T Philips Integra MR scanner (Best, the Netherlands), and a resulting resolution of 0.4 mm x 0.4 mm × 0.6 mm (interpolation was done in all 3 directions). Twenty milliliters of Omniscan (gadolinium diethylene triamine pentaacetic acid) was injected at 2.5 mL/s during the examinations. Flow rates in both vertebral arteries were measured by using phase contrast MR velocimetry. MR images were first thresholded by Amira (TGS, Inc., San Diego, CA), and resulting surface models were modified by Rapidform 2004 SP3 (INUS Technology, Seoul, South Korea). During construction of a geometric model, the surface was smoothed by Laplacian smoothing to eliminate high frequency geometric features resulting from noise or partial volume effects, but the volume of the model was preserved, and the model maintained the same geometric features. The high-frequency component of lumenal contour often gives wall shear stress estimation that is sensitive to the local contour. The final models retained the vertebral arteries, the basilar artery, and the posterior cerebral arteries.

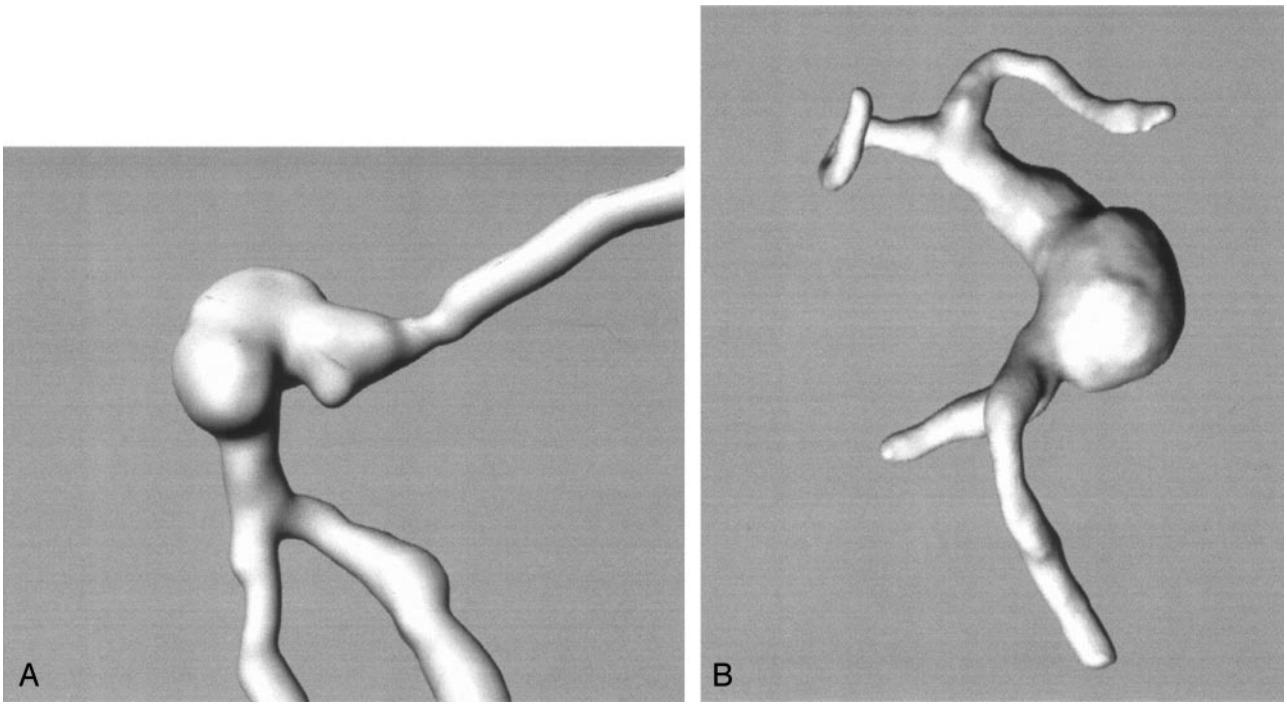

FIG 2. Models of the stable (*A*) and the growing (*B*) aneurysm.

Smaller branch vessels, which carry relatively small flow or that are distal to the sections where the velocity was measured, do not affect overall hemodynamics and were pruned at their origins (Fig 2). Aneurysmal volume was also measured on the images and from the models at different threshold level of signal intensity by 2 experienced observers. Interobserver variation was <5%.

The vasculature distal to the aneurysm in the first patient was quite irregular. Several simulations with different flow rate ratios in the posterior cerebral arteries were performed to evaluate the effect of distal vessels on flow features upstream in the aneurysm. After determining that the flow rate ratios at the posterior cerebral arteries had no influence on the flow and wall shear stress distribution within the aneurysm, the vessels distal to the aneurysm were removed and replaced by a more uniform segment to reduce computational effort that was otherwise required to accurately describe flow in those regions.

The models acquired at 2 different times were coregistered by aligning the vertebral arteries and their junction. The difference between the surfaces of the 2 models after coregistration indicates changes in aneurysm geometry. As an aneurysm grows, both the distal and proximal vasculatures are deformed. Thus, it is very unlikely that both proximal and distal vessels can be coregistered simultaneously. Coregistration of proximal vessels yields a registration error of <0.5 mm but still gives a reasonable estimation of aneurysm growth pattern.

Flow Analysis

Computational grids were generated by using GAMBIT (Fluent Inc., Lebanon, NH), and each aneurysm model had approximately 4,000,000 cells and 725,000 nodes. FLUENT (Fluent Inc., Lebanon, NH) was used to solve the Navier-Stokes equations for both steady and pulsatile flows. The fluid was assumed to be Newtonian, the flow laminar, and the vessel wall rigid. In the first patient, the flow rate through the basilar artery varied from 1 to 3.9 mL/s through the cardiac cycle with relatively equal flow through the 2 vertebral arteries, and in the second patient the flow through the basilar artery varied from 1 to 3.1 mL/s with most of the flow coming from the left vertebral artery (7). All the solutions were tested for grid independence and convergence. Because we are interested in growth between the initial imaging study and the following imaging study, the results presented in the next section are from the baseline geometry (ie, the first geometry we acquired for each patient).

Results

Figures 3*A* and -*B* are the wall shear distribution (in N/m^2) and streamlines for the aneurysm in the first patient. This aneurysm showed no change in volume with time and will be referred to as the stable aneurysm hereafter. The wall shear is seen to be slightly higher in the neck of the stenosis distal to the aneurysm. The wall shear stress is less than 2 N/m^2 on most of the aneurysm wall. There is also a clockwise vortex that dominates the flow pattern inside the aneurysm in Fig 3*B*. The projection view presented is an oblique view that is slightly rotated from coronal around the head and foot axis so the vortex can be visualized easily. The fluid enters at the midsection of the aneurysm, but there is no pronounced increase of pressure at the site of flow impact (Fig 3*C*).

In the second patient, the aneurysm that presented a significant change grew nearly 3 mm/year (Fig 4*A*). The degree of displacement of the surface from one year to the next is color coded, with blue indicating no change and red indicating maximum change. The region of growth presents at the left inferior side of the aneurysm, where the flow is slow and the wall shear stress is $<0.1 N/m^2$. The inverse of wall shear stress is plotted in Fig 4*B* and shows that the area of growth correlates with the region of low wall shear. As the aneurysm grew the distal vessels were also seen to deform in response to the change of hemo-

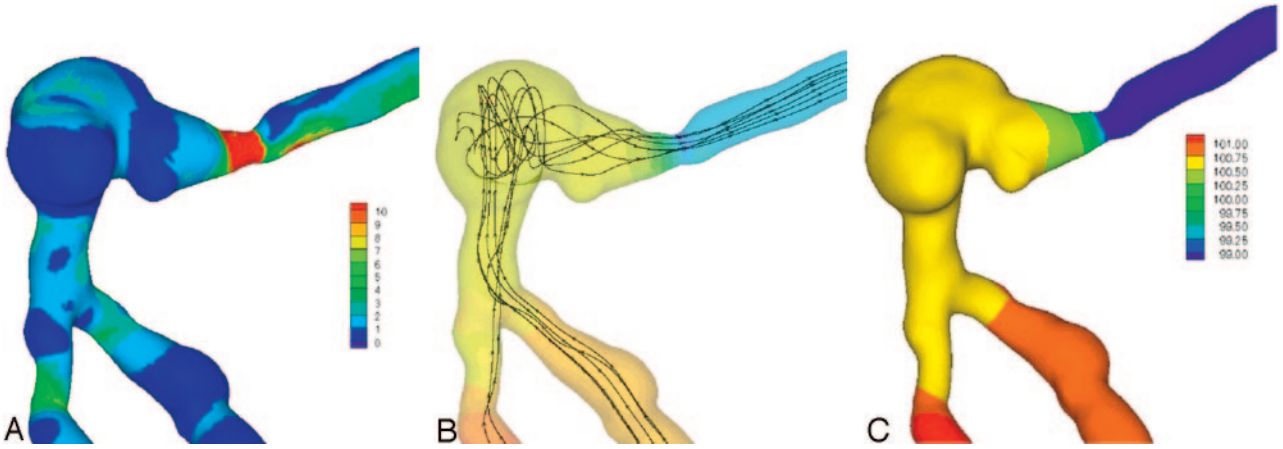

FIG 3. *A,* Wall shear stress distribution (N/m2). *B,* Streamlines in the stable aneurysm. *C,* Pressure on the aneurysm (mmHg).

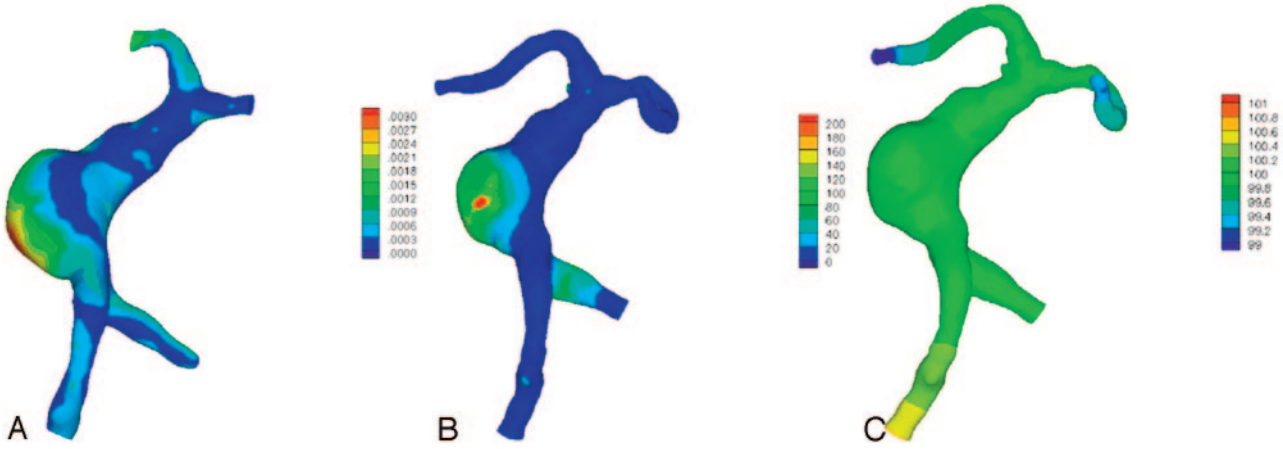

FIG 4. *A,* Change of aneurysm geometry in 2 years (m). The red indicates the location and magnitude of growth. *B,* The inverse of wall shear stress (1/[N/m^2]). *C,* Pressure distribution on the surfaces of the aneurysm and vessels (mmHg). Mean pressure was assumed to be 100 mmHg.

dynamic forces and geometry. The mean wall shear stress in a cardiac cycle was found to be similar to the level of wall shear stress for steady flow, and the oscillatory shear stress within the aneurysm was found to be very low, which indicates that the wall shear stress does not have substantial directional changes in the cardiac cycle. Numerical simulation also indicates a relatively uniform pressure within the aneurysm (Fig 4*C*) and that the pressure variation within the aneurysm was so small relative to systolic to diastolic variation that it is unlikely that pressure changes are responsible for the growth (3).

In Fig 5, histograms of wall shear stress are presented for both aneurysms for steady flow at a flow rate corresponding to end-diastole. The surface area is plotted versus the level of the wall shear stress. We note, for example, that the growing aneurysm has an area of close to 270 mm^2 where the shear stress is <0.1N/m^2, and for the stable aneurysm the surface area where the wall shear stress falls below that same value is <100 mm^2. During aneurysmal growth, the low wall shear stress area (< 0.1N/m^2) has increased from 270 mm^2 to 430 mm^2 for the growing aneurysm. Although the stable aneurysm has a smaller area with a wall shear <0.8 N/m^2, it has a larger surface area subjected to higher wall shear (>0.8 N/m^2). The total surface areas for these 2 aneurysms are quite similar: 900 mm^2 for the stable aneurysm and 1170 mm^2 for the growing aneurysm. In the growing aneurysm, there is a relatively large fraction of the surface where the wall shear is <0.1N/m^2. The stable aneurysm has a smaller surface area where the wall shear is <0.1N/m^2 and a more equally distributed wall shear over the aneurysm wall.

These trends persist when pulsatility is taken into account. The changes of wall shear over the surface of these 2 aneurysms through a cardiac cycle are shown in Fig 6. The level of wall shear is color coded. The red indicates the surface area under wall shear of 0.1 N/m^2, and the black denotes the surface area where the wall shear is high (>0.8 N/m^2). Because these aneurysms are assumed to be rigid in our model, the total surface area remains the same throughout the cardiac cycle. In the growing aneurysm, the surface area where the wall shear stress falls below 0.8 N/m^2 varies considerably between systole and diastole ($\sim$400 m^2), and variation of the surface area under the same wall shear condition is smaller for the stable aneurysm ($\sim$200 mm^2). The area where wall shear is <0.1 N/m^2 is consistently larger for the growing an-

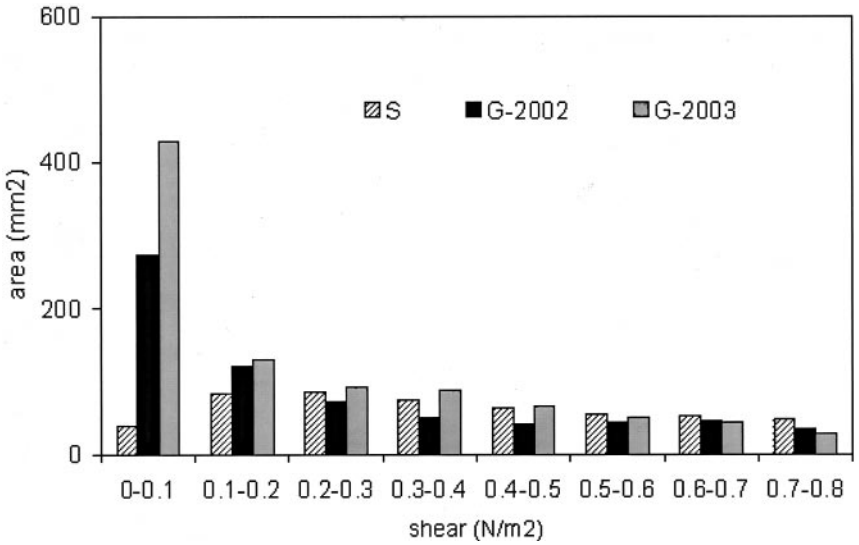

FIG 5. Histograms of the wall shear stress for the growing (*G*) and the stable (*S*) aneurysm under steady flow. The wall shear stress distributions at 2 different times (2002 and 2003) are shown for the growing aneurysm.

eurysm than for the stable aneurysm. The low wall shear area (<0.1 N/m^2) varies through the cardiac cycle from 8% to 30% of the total surface area for the growing aneurysm and only from 1% to 7% for the stable aneurysm.

Discussion

We have examined the relationship between hemodynamics and growth of 2 fusiform basilar artery aneurysms in an effort to define hemodynamic variables that may be helpful in predicting aneurysmal growth. Two basilar fusiform aneurysms of a similar size were studied. One aneurysm grew significantly, but the size of the other aneurysm remained unchanged. The largest aneurysmal growth (~3 mm/year) was found at the inferior side of the aneurysm, where the wall shear stress was very low (<0.1 N/m^2). The general flow patterns did not change with time even in the aneurysm that grew, but histograms of wall shear stress were very different in these 2 patients.

There is substantial interest in better defining the risk factors that lead to aneurysm growth and subsequent rupture. In vivo imaging and computational fluid dynamics coupled with monitoring of patients with untreated cerebral aneurysms provides a unique window into the mechanisms of aneurysm growth. These insights are important both for the natural history of untreated aneurysms but also for treated aneurysms. Longitudinal studies on the interplay of changes in aneurysm geometry and hemodynamics could permit the identification of which hemodynamic parameters are important and may shed light on the process of aneurysm development. A better understanding of this process will provide guidance on when to intervene in a given patient and will facilitate the optimization and analysis of current treatments and devices.

Cerebral aneurysms are thicker and less compliant (11, 12); their motions are not detectible by our current imaging procedure, and neither are the motion of adjacent vessels. The rigid wall assumption is a limitation of our study, though previous study has demonstrated that wall motion is of secondary importance (13).

In this report, the axial diameter of the aneurysm grew from 10.6 mm to 13.3 mm. Changes of that order are substantially larger than any variations in image-derived lumenal size or any possible coregistration errors, which are typically of the order of a single voxel. Therefore, the geometric difference denotes true aneurysm growth.

Each simulation was performed by using the frequency we measured on each individual. The aneurysm that was seen to grow was in a patient who had a slightly longer cardiac cycle (0.96 seconds) and carried a lower flow rate (3.1 mL/s at peak systole) than did the stable aneurysm (0.84 seconds and 3.9 mL/s at peak systole, respectively), but the waveforms were very similar. The difference in heart rate appears not to be an important contributor to the difference in wall shear stress distribution, because in each case the mean wall shear in a cardiac cycle is similar to the wall shear stress distributions for steady flow. A large low wall shear area appeared consistently within the aneurysm throughout the cycle in the growing aneurysm. Anatomic differences clearly dictate the flow pattern and wall shear distribution.

It is often speculated that the location of aneurysm growth is most likely to be at the location where the impact from the incoming flow is at its highest (1). Our results, however, show that aneurysm growth does not necessarily occur at the site of flow impingement, where the pressure might be slightly higher than elsewhere. The pressure increase resulting from flow impact is only a fraction of the pressure variation during a cardiac cycle and may not be sufficiently significant to introduce aneurysms or stimulate their growth.

The perianeurysmal environment might provide constraints that limit growth in a certain direction and permit growth in other direction (14, 15). It is shown that the surrounding material may stabilize the aneurysm (15). The influences of perianeurysmal environment, however, are neglected in light of the difficulty

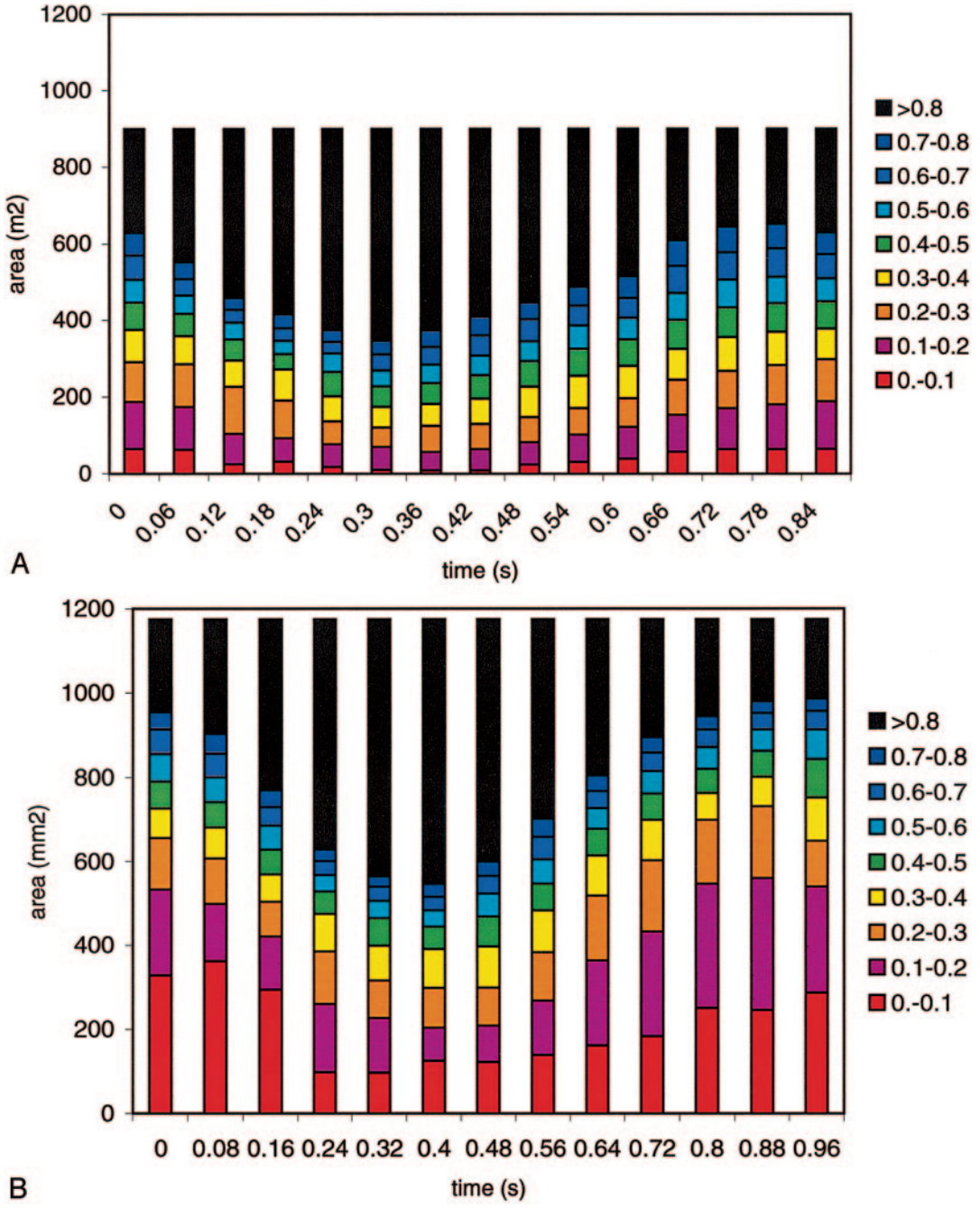

FIG 6. Influence of pulsatility on the wall shear stress distribution for the stable (*A*) and the growing (*B*) aneurysm. Colors indicate the level of wall shear to which the aneurysm wall is subjected.

of defining surrounding structures on contrast enhanced MR angiographs.

This study also found a relatively uniform pressure distribution over the aneurysm wall, which indicates that the pressure might also have little to do with rapid aneurysm development. Although aneurysm growth occurred at the caudal aspect of the aneurysm, a lateral growth pattern implies that gravity was not an important factor. It is possible, in both cases, that the initial aneurysm development may have been a result of a local weakness in the arterial wall. Details of geometric difference between the 2 patients, however, could have led to a situation where an extensive region of low wall shear stress developed results in an interruption of the normal protective functioning of the endothelium. It has been well documented that the wall shear regulates the function of endothelial cells (16, 17). Although the specific role of endothelial cells is uncertain in aneurysm development, it could be hypothesized that the endothelial cell, mediated by wall shear stress, is important in vessel wall degeneration and aneurysm growth. Prolonged exposure of low wall shear leads to cell death via apoptosis (17–19), and abnormal wall shear often results in vascular and cerebrovascular diseases. Fragmentation of internal elastic lamina and apoptosis of medial

smooth muscle cells are often associated with aneurysm formation (20). Our study agreed with a recent study reported by Shojima et al (21) in which the wall shear stress at middle cerebral aneurysms was found lower than the wall shear stress at vessel region.

Fusiform aneurysms are commonly related to intracranial atherosclerosis (22). Both aneurysms presented in this report have a stenosis near the aneurysm: the stenosis appears distal to the aneurysm in the first case and proximal to the aneurysm in the second case. Because it is well known that the wall shear stress plays a very important role in atherosclerosis (23, 24), it is not surprising that there is a significant difference in wall shear stress distribution in these 2 cases, though it is unclear whether the close proximity of the stenosis to the aneurysm is only coincidental (7). Although the comparison presented here between 2 patients, each with fusiform basilar aneurysms, is suggestive of factors that might differentiate between aneurysms that tend to grow and those that remain stable, firm conclusions would require similar demonstration of this effect in a much wider population.

Although the 2 subjects discussed here presented with important differences in their clinical histories, computational modeling views the flow channel as a rigid wall and only attempts to account for the influence of hemodynamic factors within that limited framework. An early study by Nakatomi et al (25) has shown that asymptomatic aneurysms were often smaller than symptomatic aneurysms. Therefore, 2 aneurysms of similar size were selected for this study, and they may represent 2 aneurysms at a similar developmental stage. Large and small aneurysms may have very different pathophysiologic conditions that may predispose them for growth. Other factors might well play an important role in the evolution of aneurysms, but these computational methods applied in longitudinal studies of aneurysmal disease should prove helpful in evaluating, on an individual basis, which regions in a specific aneurysm might be at risk for subsequent growth. Knowledge of that kind could be helpful in determining which interventions—surgical, endovascular, or pharmacologic—might be most effective in a given situation.

This report describes an approach to analyzing and confirming the impact that flow dynamics might have in the progression of intracranial aneurysms. If a relationship between wall shear stress and aneurysm growth were established, predictions of future aneurysm growth and loading could be made. Predictions that the wall tension had increased and was approaching the breaking point of the vessel would increase the urgency to intervene. Similarly, an inference that mass effect, and concomitant symptoms, from a growing aneurysm were likely to worsen might also provide an important criterion in the medical treatment algorithm.

Acknowledgments

We are grateful for financial support from the National Institute of Health (grant NS-37921). We also acknowledge the assistance of Nancy Quinnine, RN.

References

1. Hassan T, Ezura M, Timofeev EV, et al. **Computational simulation of therapeutic parent artery occlusion to treat giant vertebrobasilar aneurysm.** *AJNR Am J Neuroradiol* 2004;25:63–68
2. Lieber BB, Livescu V, Hopkins LN, Wakhloo AK. **Particle image velocimetry assessment of stent design influence on intra-aneurysmal flow.** *Ann Biomed Eng* 2002;30:768–777
3. Lieber B, Gounis M. **The physics of endoluminal stenting in the treatment of cerebrovascular aneurysms.** *Neurol Res* 2002;24: S33–S42
4. Hoi Y, Meng H, Woodward SH, et al. **Effects of arterial geometry on aneurysm growth: three-dimensional computational fluid dynamics study.** *J Neurosurg* 2004;101:676–681
5. Steinman DA, Milner JS, Norley CJ, et al. **Image-based computational simulation of flow dynamics in a giant aneurysm.** *AJNR Am J Neuroradiol* 2003;24:559–566
6. Foutrakis GN, Burgreen G, Yonas H, Sclabassi RJ. **Construction of 3-D arterial volume meshes from magnetic resonance angiography.** *Neurol Res* 1996;18:354–360
7. Jou LD, Quick CM, Young WL, et al. **A computational approach to quantifying hemodynamic stress in giant cerebral aneurysms.** *AJNR Am J Neuroradiol* 2003;24:1804–1810
8. Yim PJ, Cebral JJ, Mullick R, Marcos HB, Choyke PL. **Vessel surface construction with a tubular deformable model.** *IEEE Trans Med Imaging* 2001;20:1411–1421
9. Long Q, Xu XY, Collins MW, Bourne M, Griffith TM. **Magnetic resonance image processing and structured grid generation of a human abdominal bifurcation.** *Comput Methods Programs Biomed* 1998;56:249–259
10. Long Q, Ariff B, Zhao SZ, et al. **Reproducibility study of 3D geometrical reconstruction of the human carotid bifurcation from magnetic resonance images.** *Magn Reson Med* 2003; 49:665–674
11. Toth M, Nadasy GL, Nyar I, et al. **Are there systemic changes in the arterial biomechanics of intracranial aneurysm patients?** *Pflugers Arch* 2000;439:573–578
12. Wilson K, Whyman M, Hoskins P, et al. **The relationship between abdominal aortic aneurysm wall compliance, maximum diameter and growth rate.** *Cardiovasc Surg* 1999;7:208–213
13. Perktold K, Rappitsch G. **Computer simulation of local blood flow and vessel mechanics in a compliant carotid artery bifurcation model.** *J Biomech* 1995;28:845–56
14. San Millan Ruiz D, Tokunaga K, Dehdashti AR, et al. **Is the rupture of cerebral berry aneurysms influenced by the perianeurysmal environment?** *Acta Neurochir* 2002;82:31–34
15. Seshaiyer P, Humphrey JD. **On the potentially protective role of contact constraints on saccular aneurysms.** *J Biomech* 2001; 34:607–612
16. Chen S. **Molecular and mechanical bases of focal lipid accumulation in arterial wall.** *Progr Biophys Mol Biol* 2003;83:131–151
17. Resnick N, Yahav H, Shay-Salit A, et al. **Fluid shear stress and the vascular endothelium: for better and for worse.** *Prog Biophys Mol Biol* 2003;81:177–199
18. Sho E, Sho M, Singh TM, et al. **Blood flow decrease induces apoptosis of endothelial cells in previously dilated arteries resulting from chronic high blood flow.** *Arterioscler Thromb Vasc Biol* 2001;21:1139–1145
19. Sho E, Nanjo H, Sho M, et al. **Arterial enlargement, tortuosity, and intimal thickening in response to sequential exposure to high and low wall shear stress.** *J Vasc Surg* 2004;39:601–612
20. Kondo S, Hashimoto N, Kikuchi H, et al. **Apotosis of medial smooth muscle cells in the development of saccular cerebral aneurysms in rats.** *Stroke* 1998;29:181–189
21. Shojima M, Oshima M, Takagi K, et al. **Magnitude and role of wall shear stress on cerebral aneurysm: computational fluid dynamic study of 20 middle cerebral artery aneurysms.** *Stroke* 2004;35: 2500–2505
22. Vates GE, Auguste KI, Lawton ML. **Fusiform, dolichoectatic, and dissecting aneurysms: diagnosis and management.** In: *Management of cerebral aneurysms.* Le Roux PD, Winn HR, Newell DW, eds. Philadelphia: Saunders;2004:689–710
23. Davies PF. **Flow-mediated endothelial mechanotransduction.** *Physiol Rev* 1995;75:519–560
24. Malek AM, Alper SL, Izumo S. **Hemodynamic shear stress and its role in atherosclerosis.** *JAMA* 1999;282:2035–2042
25. Nakatomi H, Segawa H, Kurate A, et al. **Clinicopathological study of intracranial fusiform and dolichoectatic aneurysms: insight on the mechanism of growth.** *Stroke* 2000;31:896–900